Closed Orbit Injection of Ions in a Magnetic Mirror Field

W. Dommaschk, H.B. Schilling, P. Ulbricht

IPP 0/6 December 1970

MAX-PLANCK-INSTITUT FÜR PLASMAPHYSIK

GARCHING BEI MÜNCHEN

MAX-PLANCK-INSTITUT FÜR PLASMAPHYSIK

GARCHING BEI MÜNCHEN

Closed Orbit Injection of Ions in a Magnetic Mirror Field

W. Dommaschk, H.B. Schilling, P. Ulbricht

IPP 0/6 December 1970

Die nachstehende Arbeit wurde im Rahmen des Vertrages zwischen dem Max-Planck-Institut für Plasmaphysik und der Europäischen Atomgemeinschaft über die Zusammenarbeit auf dem Gebiete der Plasmaphysik durchgeführt.

IPP 0/6

W. Dommaschk
H.B. Schilling
P. Ulbricht

Closed orbit injection of ions in a magnetic mirror field (Dec. 1970)

Abstract

In order to inject ions from outside into the electron ring accelerator instead of generating them by ionization with the relativistic electrons, a device for closed orbit trapping of ions in a magnetic mirror field was investigated. With a pulsed duoplasmatron ion source and a pulsed electric inflector 10^{10} monoenergetic 3.75 keV protons were trapped in a circle of 19 cm major radius and 2 cm minor radius. The magnetic field was 480 G and the field index 0.5 at the major radius. Single-turn inflection was used, i.e. protons injected into this field during the revolution time of 1.4 μsec were trapped by removing the electric inflector fields in about 200 nsec. Up to 15 revolutions of the trapped ions were observed at a pressure of 2×10^{-5} torr by means of electric probe signals due to azimuthally asymmetric charge density variations in the ion ring. The number of trapped ions was obtained by electrically deflecting the ions towards a capacitively grounded collector as a function of the trapping time.

Summary: Page:

1. Introduction 1

2. Theory 2

2.1 Ion energy and injection current 2

2.2 Beam spread due to space charge 3

2.3 Cross section of the injected ion beam 4

2.4 Beam inflection 6

2.5 Reduction of the longitudinal ion energy during electron injection 11

2.6 Reduction of the ion betatron amplitudes after electron injection 12

2.7 Nonadiabatic compression of the ion ring 13

3. Experiment 16

3.1 Experimental setup 16

3.2 Systems for pulsed operation 19

3.21 Duoplasmatron pulsing 19

3.22 Beam chopper 19

3.23 Inflector power supply 20

3.24 Ring azimuthal irregularity probe 20

3.25 Ion ring deflection 21

3.26 Pulse flow diagram 21

3.3 Emission properties of the ion source 23

3.4 Beam guiding 25

3.5 Quality of the injected proton beam 27

3.6 Trapping and detection of the ion ring 29

3.7 Measurement of the trapped ion number 30

4. References 33

1. Introduction

For some years attempts have been made to develop the so-called electron ring accelerator (ERA), which should be able to accelerate ions electrically trapped in a relativistic electron ring up to very high energies by axially accelerating the electron ring [1, 2, 3]. The electron ring with a major radius of about 3 cm and a minor radius of about 1 mm is obtained from a larger electron ring of about 20 cm major radius, which should contain about 10^{13} 2 MeV electrons, by compressing it in a magnetic mirror field in about 10 μsec. The large ring is obtained by closed orbit injection of the electrons from outside into the uncompressed mirror field. To get the right holding power for the ions and the right effective mass of the ring, the ion number should be a certain small fraction of the electron number. The commonly proposed way of obtaining the ions is to ionize neutral gas by the relativistic electrons in the compressed ring. An alternative way is to inject both electrons and ions from outside with the proper canonical momentum into the same ring and to compress this combined electron ion ring. This would have the advantage that the self-focusing effect would already begin to act during compression. Since the electron velocity in the ring is some hundred times greater than the ion velocity, the ion ring must be generated first and then the electrons should be injected into the ion ring. Both the electric and magnetic fields of the electrons should have a trapping effect on the ions, diminishing their mean betatron oscillation amplitudes though their oscillation energy is increased.

To study the conditions for injecting ions as described, a device for injecting the ions in a static field was proposed [4]. Preliminary results obtained with the partially completed experiment were given in [5]. In the following the final con-

ditions and results shall be presented together with a description of the apparatus, electronic accessories, and measurements.

2. Theory

2.1 Ion energy and injection current

The ion ring and the electron ring are generated at the same major radius in the same field. They must therefore be oppositely injected with equal momentum per unit charge. Since the ion velocities can be assumed as nonrelativistic in this case, it follows from $m_i v_i/Z = \beta\gamma m_e c$ that:

$$U_i = (\gamma^2-1)Zm_e^2c^2/2em_i \quad = 139(\gamma^2-1)Z/A \quad [V]$$

$$v_i = \sqrt{\gamma^2-1}\, Zm_e c/m_i \quad = 1.63 \times 10^7\sqrt{\gamma^2-1}\, Z/A \quad [cm/sec] \quad (1)$$

where $\gamma = 1 + U_e/5.12 \times 10^5\ V$

Here $m_i=m_pA$, m_p, m_e are the ion, proton and electron rest masses, e is the electron charge, Z, A are the ionic charge and mass number, c, v_i are the velocity of light and the ion velocity in cm/sec, U_e, U_i are the values of the acceleration voltages in volts for electrons and ions, and $\gamma = 1/\sqrt{1-\beta^2}$ is the relativistic mass ratio for the electrons. For U_e = 2.2 MV, i.e. $\gamma = 5.3$, and for protons (A=Z=1) we get U_i = 3.75 kV and $v_i = 8.5 \times 10^7$ cm/sec. At a major radius of 19 cm the revolution time for the protons is 1.4 µsec and for electrons 4 nsec. So the protons move only about 3 mm during one revolution of the electrons.

The desired number of ions in the ring has to be injected during one single revolution. For reasons that become clear later

multiturn injection of the ions did not seem appropriate. The injection current is then given by:

$$I_i = \sqrt{\gamma^2-1}\, m_e c N_i e Z^2/2\pi R m_i = 4.16 \times 10^{-13} \sqrt{\gamma^2-1}\, N_i Z^2/AR \quad (2)$$

[A]

Here N_i is the number of ions in the ring and R the major ring radius. For $N_i = 10^{10}$ and R = 19 cm we get with the foregoing numbers for protons I_i = 1.1 mA. This number has to be slightly corrected since the ring is not filled completely during the single-turn injection. As can be seen from eq. (2), the current increases with the square of the charge number and decreases with increasing mass number. Since the total number of elementary charges in the ring is to be treated as constant rather than the ion number, the current requirements should increase only as the first power of Z.

2.2 Beam spread due to space charge

If no space charge compensation and no external fields are present, a rotational symmetric homogeneous ion beam with zero emittance increases its radius according to the formula [6]:

$$x/r_o = (KU_i^{3/4} I_i^{-1/2}) \int_0^{\sqrt{\ln(r/r_o)}} \exp(\xi^2)\, d\xi \quad (3)$$

Here r_o is the beam radius in the beam waist and r is the radius at the axial distance x from the waist of the beam under the condition that $dr/dx \ll 1$. The factor K is given gy:

$$K = (8\pi\varepsilon_o (2eZ/m_i)^{1/2})^{1/2} = 1.76 \times 10^{-3} (Z/A)^{1/4}$$

$$[A^{1/2}/V^{3/2}]$$

For the distance x_2 where the beam radius has doubled ($r=2r_o$) the value of the integral is given in [5] as 1.0754. This yields:

$$x_2/r_o = 1.89\times10^{-3}U_i^{3/4}/I_i^{1/2}$$

$$\text{with (2):} \quad = 2.92\times10^{3}U_i^{3/4}A^{1/4}R^{1/2}/Z^{3/4}N_i^{1/2}(\gamma^2-1)^{1/4} \qquad (4)$$

$$\text{with (1):} \quad = 1.19\times10^{5}(\gamma^2-1)^{1/2}R^{1/2}/N_i^{1/2}A^{1/2}$$

For protons guided at the injection voltage this yields with our foregoing numbers $x_2=26r_o$. To get better values the guiding voltage must therefore be higher than the injection voltage. If N_iZ is taken as constant, then we see from the second line of eq. (4) that x_2 increases in proportion to $(A/Z)^{1/4}$, e.g. the beam guiding for heavier or multiply charged ions should be even easier than for protons. At places where the beam must be guided approximately at the desired injection voltage given by eq. (1) we see, however, from the third line of eq. (4) that x_2 changes as $(Z/A)^{1/2}$. For heavy ions this is a serious problem if no space charge compensation is possible.

2.3 Cross section of the injected ion beam

In order to prevent the minor cross section of the ion ring from oscillating inside the magnetic mirror field, the phase space ellipse of the injected beam must coincide with the equilibrium phase space ellipse of the ion ring. The injected beam must therefore have a waist at the injection point, where it turns off into the circular path, and the cross section of this waist must coincide with the equilibrium cross section of the ring. To get this cross section we assume for simplicity that the field index at the major ring radius is about $n \approx 1-n \approx Q^2 \approx 0.5$. The minor equilibrium cross section can then be considered as circular. We assume the minor ring radius to be small relative to the major radius and neglect the effect of the torus form on the electric space charge field. We further assume that the

charged particle density is constant inside the minor ring cross section and zero outside. Then the defocusing and focusing forces F_d, F_f acting on an ion are:

$$F_d = rN_i e^2 Z^2 p/4\pi^2 \varepsilon_o r_i^2 R \qquad (5)$$

$$F_f = -reZQ^2 v_i B/R = -reZQ^2 . 2U_i/R^2 = -rm_i \omega_c^2 Q^2 \qquad (6)$$

Here r is the radial or axial deviation of an ion from the midpoint of the minor ring cross section and r_i is the minor ring radius. $p \leq 1$ is a neutralization factor due to slow electrons generated, for example, by rest gas ionization. ε_o is the vacuum dielectric constant, B is the magnetic field at the major radius and ω_c the corresponding cyclotron frequency of the ions. Then from (5,6) the equation for the betatron oscillations of the ions must be of the form:

$$\ddot{r} = -r\omega_c^2 Q^2 \left\{ 1 - r_{io}^2/r_i^2 \right\} \qquad (7)$$

With no betatron oscillations present, i.e. if the ring emittance is zero, we have $\ddot{r} = 0$ or $r_i = r_{io}$, where from (5,6):

$$r_{io}^2 = KZN_i Rp/Q^2 U_i = 1.65 \times 10^{-10} N_i RpA/Q^2 (\gamma^2 - 1) \; [cm^2] \qquad (8)$$

Here $K = e/8\pi^2 \varepsilon_o = 2.3 \times 10^{-8}$ Vcm and r_{io} is the minor ring radius at zero emittance. For our proton example we get $r_{io} = 1.5$ cm. If $N_i Z$ is considered constant, then r_{io} is proportional to $(A/Z)^{1/2}$. The injection of heavy ions is therefore impossible without space charge compensation or some means of electric focusing as proposed, for example, in [4] .

If the emittance is not zero, then r_i becomes greater than r_{io}. The largest occurring betatron amplitudes defining the ring

cross section and the ring emittance are then equal to r_i. The ring emittance is $\varepsilon = \pi r_i^2 Q_1/R$, where Q_1 is the betatron frequency divided by ω_c, as given by eq. (7). So we get:

$$\varepsilon = r_i^2 Q(1-r_{io}^2/r_i^2)^{1/2}/R \qquad (9)$$

Since $\varepsilon\sqrt{U_i}$ is constant, ε is known from the beam emittance and we get from eq. (9) for the new equilibrium ring radius r_i at nonzero emittance:

$$r_i^2 = (1 + (1 + 4(\varepsilon R/r_{io}^2 \pi Q)^2)^{1/2})r_{io}^2/2 \qquad (10)$$

where r_{io} is given by eq. (8). From emittance measurements (sec. 3.4) we have $\varepsilon \approx 200$ mrad cm for a 4 keV proton beam. This yields $r_i \approx 1.75$ cm for our proton example. Since this value is rather large, single-turn injection was used in our device instead of multiturn injection.

2.4 Beam inflection

In order to prevent the injector snout from distorting the magnetic field near the ion ring, it had to be drawn back from the injection plane (see Fig. 2), where the beam enters the circular path. To guide the beam from the snout to this point electric fields generated by suitably shaped electrodes shall be used to compensate approximately the magnetic forces and give a nearly straight beam. The field strength required at the beam axis is then not greater than $2U_i/R$. This is about 400 V/cm for our proton beam. The condition that the components of the Lorentz field $\mathcal{E} + \mathbf{v}\times\mathcal{B}$ normal to the beam axis should vanish cannot be exactly fulfilled since $\nabla\times\mathcal{E} = 0$, but $\nabla\times(\mathbf{v}\times\mathcal{B})$ is not zero in general. Even if $\mathcal{E}$ and $\mathcal{B}$ were homogeneous and

normal to the beam axis and to each other, no exact cancellation of forces is possible. If the Lorentz field is made zero in this case for an ion propagating along the beam axis, this field acts as a cylinder lens for ions propagating beside the axis. Since the value of the velocity vector $\mathfrak{v}$ increases in the direction of the electric field vector, a focusing action in the plane normal to the magnetic field results. To reduce this effect, $\mathfrak{E}$ must increase its value in its own direction and/ or $\mathfrak{B}$ must decrease its value in the same direction. Either alternative, however, now produces focusing in the plane normal to the electric field vector.

For our inflector we choose the beam energy to be constant at the beam axis and equal to the injection energy. At the axis the electric field must then be normal to this axis and to the magnetic field. Furthermore, the value of the electric field at the axis must change proportionally to the magnetic field. To get the focusing properties and conditions for the inflector, we choose Cartesian coordinates for the position of an ion near the axis (Fig. 1a). Here x is its position along the beam axis, y its deviation from this axis in the direction of the main electric field, and z its deviation in the direction of the main magnetic field. At the axis we have:

$$R_c = m_i v_i / Be\mathfrak{z} = 2U_i / E \qquad (11)$$

Where R_c is the x-dependent cyclotron radius 1) at the axis in the pure magnetic field B. The right side of eq. (11) is the condition for the electric field $\mathfrak{E}$ that an ion moving along the axis is not deflected. R_c is equal to R in the injection plane $\mathfrak{P}$ (Fig. 1a) and greater than R in the inflector. If $\mathfrak{r} = (0,y,z)$

---

1) R_c is not identical with the R_c-value given in eq.(4) in [5].

is a vector indicating the deviation of an ion from the x-axis, then the paraxial ray equation for $\mathbf{r}$ in our case is:

$$\mathbf{r}'' = \frac{eZ}{m_i v_i}\left(\mathcal{E}/v + \mathbf{u} \times \mathcal{B}\right)_{\perp} \qquad (12)$$

where quantities of second and higher orders in distance from and slope to the x-axis are neglected. The primes denote differentiation with respect to x, v is the velocity of the ions near the axis, which is constant and equal to v_i at the axis, and $\mathbf{u}$ is a normal vector in the direction of the ion velocity. The $\perp$ sign indicates that only the components normal to the x-axis are taken. The quantities $\mathcal{E}$, v_i, U_i, $\mathbf{u} \times \mathcal{B}$ shall

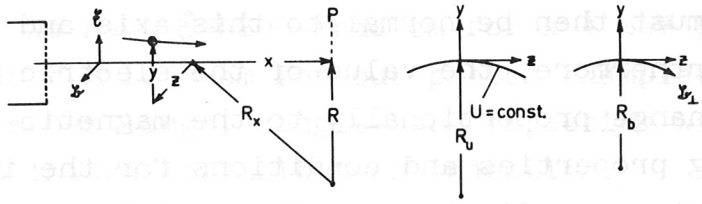

Fig.1: Definition of coordinates and parameters for beam inflection.

be expressed by a first-order Taylor expansion around the axis. The first-order quantities of the components E_y, E_z, B_y, B_z of the electric and magnetic fields near the axis are thereby expressed in terms of the x-dependent radii of curvature $R_b = -B/(\partial B_z/\partial y)$ and $R_u = -E/(\partial E_y/\partial y)$ at the x-axis and in their y-z projection according to Fig. 1b. Their values are positive if the centre of curvature lies on the negative y-axis as drawn in the figure. The value of R_b may be expressed by the x-dependent magnetic field index $n_x = -R_x \partial B_z/\partial R_x B$, where R_x is the distance between the magnetic main field axis and the x-projection of the ion (see Fig. 1a):

$$R_b = R_x^2/n_x R \qquad (13)$$

We make use of $\nabla\times\mathfrak{B} = \nabla\times\mathfrak{E} = 0$, $\nabla\mathfrak{B} = 0$ and of the fact that the x-y plane is a symmetry plane. We consider only the focusing action produced by the inflector electrode potentials. Space-charge effects can be added separately in an approximate manner (see below). Thus we use $\nabla\mathfrak{E} = 0$, where the contribution of the E_x-component can be neglected as of second order in z. In first order we get the following expressions near the x-axis, with $\mathcal{U}>0$ as the negative acceleration voltage:

$$U = U_i + Ey; \quad E_y = E(1-y/R_u); \quad E_z = Ez/R_u;$$

$$1/v = 1/v_i(1+Ey/2U_i) = (1-y/R_c)/v_i;$$

$$B_y = -Bz/R_b; \quad B_z = B(1-y/R_b); \tag{13a}$$

$$\mathfrak{E}_\perp/v = (E/v_i)\,(0, 1-y/R_u-y/R_c, z/R_u);$$

$$(\mathfrak{n}\times\mathfrak{B})_\perp = (0, z'B_x-B_z, B_y-y'B_x) = B(0, y/R_b-1, z/R_b)$$

The first order quantities y', z' give no contribution in first order, because they appear only in combination with B_x, which is of first order in z. From eqs. (11), (12),(13a) we get:

$$y'' = -y(1/R_u-1/R_b+1/R_c)/R_c \tag{14}$$

$$z'' = -z(1/R_b-1/R_u)/R_c \tag{15}$$

Here R_c, R_b, R_u are all functions of x. At the injection plane P (see Fig. 1a) we assume that the electric field is made to vanish, i.e. stray-field effects at the end of the inflector are ignored. Here the ion paths go over into the pure magnetic mirror field, whose focusing forces with respect to the equilibrium orbit with radius R are described by the well-known betatron oscillation equations:

$$d^2r/ds^2 = -r(1-n)/R^2 \tag{16}$$

$$d^2z/ds^2 = -zn/R^2 \tag{17}$$

Here s is the arc length along the equilibrium orbit, r is the radial deviation from the equilibrium orbit, z the deviation in the direction of the magnetic field axis and n the field index on the equilibrium orbit. In the injection plane P z in eq. (17) is therefore equal to z in eq. (15), r = y and ds = dx, since the x-axis shall be tangential to the equilibrium orbit in this plane.

Optimum adaption of the inflector to the magnetic mirror field is achieved if the ratio (1-n)/n obtained from the right sides of eqs. (16), (17) equals the corresponding ratio obtained from eqs. (14), (15). This yields for R_u the condition:

$$1/R_u = 1/R_b - n/R_c \tag{18}$$

The inflector potential at the x-axis is now specified by its value, its first derivatives with respect to y and z, and its second derivative with respect to y. As can be seen from the power expansion of an electrostatic potential subject to $\Delta U = 0$ given in [8], these values can indeed be prescribed by four independent functions of x. With condition (18), we obtain from eqs. (14), (15):

$$y'' = -y(1-n)/R_c^2 \tag{19}$$

$$z'' = -zn/R_c^2 \tag{20}$$

At the injection plane P, where $R_c = R$, these equations are identical with eqs. (16), (17), and so condition (18) provides the most steady transition from the inflector to the mirror field. Since $R_b = R/n$ at this plane, we have $R_u = \infty$ there, i.e. the electric field should be homogeneous at this plane. In our device a magnetic field with n=0.5 at the equilibrium orbit was chosen. The R_c-values obtained from this magnetic field give R_u-values above 80 cm along the inflector, i.e.

a nearly uniform electric field. A corresponding inflector electrode configuration as designed with the aid of relaxation methods is given in Sec. 3.4.

Comparison of eqs. (19), (20) with (16), (17) shows that the inflector, if adapted to the magnetic mirror field by eq. (18), focuses somewhat more weakly than the magnetic mirror. The distances between nodes in the mirror as obtained from eqs. (16) and (17) are $\pi R/\sqrt{1-n}$ and $\pi R/\sqrt{n}$ respectively. In the inflector we have from eqs. (19), (20) similar expressions with the mean value $\overline{R}_c$ instead of R, which is about 10 or 20 per cent larger than R in our device.

To get approximately the beam envelope under the influence of space charges and the finite emittance inside the inflector, the differential equations for the beam spread given in [9] may be combined with eqs. (19), (20).

2.5 Reduction of the longitudinal ion energy during electron injection

During the electron injection the electron and ion momenta are reduced by an azimuthal electric field induced by the increasing ring current. Since the ion revolution time is very long compared with the electron injection time, the sudden ion energy reduction induces betatron oscillations of the ions. By integrating $eL\dot{I}_e/2\pi R = -m_i\dot{v}_i$, where L is the mean ring inductance and $\dot{I}_e$ the time variation of the electron current, an approximation of the ion energy change may be obtained. Assuming homogeneous space charge distribution, neglecting the ion charge, and dividing the energy change by the approximate electrostatic potential energy difference in the electron ring, we get the ratio $2\,Lcv_i\,\varepsilon_o/R$. This is small relative to unity since $L \approx 10^{-6}$ Hy in our case. The ion betatron amplitudes caused by this effect are therefore small relative to the small electron ring radius and can be neglected.

2.6 Reduction of the ion betatron amplitudes after electron injection

Before the electrons are injected, the ions oscillate about the duty circle approximately according to $\ddot{r}_1 = -\omega_c^2 Q_1^2 r_1$, where Q_1^2 is the factor of $-r\omega_c^2$ at the right side of eq.(7). After the electron injection the ions oscillate approximately according to $\ddot{r}_2 = -\omega_c^2 Q_2^2 r_2$, where:

$$Q_2^2 \approx Q_1^2 + eRN_e/8\pi^2 \varepsilon_o r_e^2 U_i \qquad (21)$$

Here N_e is the electron number in the ring and r_e is the minor electron ring radius, which is assumed to be about equal to r_i. Since $Q_1 < 1$ and $N_e \gtrsim 10^{12}$, we have $Q_1^2/Q_2^2 \ll 1$. The transition $Q_1 \rightarrow Q_2$ occurs very quickly compared with the ion oscillation time. It can therefore be idealized by a simple step at the time t = 0. Immediately before and after the step r and $\dot{r}$ must have the same values. If $r_1 = a_1 \sin(\omega_c Q_1 t + \delta_1)$ and $r_2 = a_2 \sin(\omega_c Q_2 t + \delta_2)$ are the solutions before and after the step, we get:

$$a_1 \sin(\delta_1) = a_2 \sin(\delta_2)$$

$$a_1 Q_1 \cos(\delta_1) = a_2 Q_2 \cos(\delta_2) \qquad \text{or}$$

$$\overline{a_2^2} = a_1^2 (1 + Q_1^2/Q_2^2)/2 \qquad (22)$$

Here $\overline{a_2^2}$ is the mean value of a_2^2 with respect to the equally distributed phase angles δ_1. After the electron injection the mean ion density in the ring is therefore approximately doubled.

In an adiabatic process the oscillation energy changes proportionally to the frequency $a^2\omega^2/2 \sim \omega$ or $a_2^2 Q_2 = a_1^2 Q_1$, i.e. the emittance which is proportional to $a^2 Q$ remains constant if the longitudinal energy is not changed. From eq. (22), however, which describes a nonadiabatic transition, the emittance can be seen to be increased by the mean factor $(Q_2/Q_1 + Q_1/Q_2)/2$. This may be several times larger than unity.

2.7 Nonadiabatic compression of the ion ring

The compression of the combined electron ion ring has to take place in about ten or twenty microseconds. During this time the ions make only a small number of revolutions. To determine to what extent the ion compression can be looked at as an adiabatic process, their compression shall be calculated without using the adiabatic invariant directly. We use the Lagrange function $L = m_i c^2(1-(1-\beta^2)^{1/2}) + q\mathfrak{A}\mathfrak{v}$, where $\mathfrak{A}\mathfrak{v} = (0,A,0)\cdot(\dot{\varrho},\varrho\dot{\varphi},0) = A\varrho\dot{\varphi}$, $\beta^2 = (\dot{\varrho}^2+\varrho^2\dot{\varphi}^2)/c^2$ and $q > 0$ is the ion charge. The magnetic vector potential is related to the magnetic field by $\mathfrak{B} = \nabla\times\mathfrak{A}$. In our case only the φ - component $A_\varphi = A$ of $\mathfrak{A}$ is different from zero. The quantities $\dot{\varrho}$ and $\varrho\dot{\varphi}$ are the radial and azimuthal velocity components of an ion, where ϱ is the radial distance from the magnetic field axis. The axial velocity component was taken to be zero and forces between particles are ignored. From the Lagrangian equations of motion it follows that:

$$d(m_i\gamma\dot{\varrho})/dt = q\dot{\varphi}(A+\varrho\,\partial A/\partial\varrho)+m_i\gamma\varrho\dot{\varphi}^2 \qquad (23)$$

$$\varrho(m_i\gamma\dot{\varphi}\varrho+qA) = p_\varphi = \text{const.} \qquad (24)$$

Before the compression we assume $\dot{\varrho} = 0$, i.e. no betatron oscillations. Then the right side of eq. (23) is zero at this time, i.e. $m_i\gamma\varrho\dot{\varphi}_o = -q(A+\varrho\partial A/\partial\varrho)_o$. The index o indicates conditions preceding the compression. Inserting $\dot{\varphi}_o$ in eq.(24) yields:

$$p_\varphi = -q(\varrho^2\partial A/\partial\varrho)_o \qquad (25)$$

Elimination of $\dot{\varphi}$ from (23,24) gives:

$$d(\gamma\dot{\varrho})/dt = \frac{p_\varphi^2}{m_i^2\gamma\varrho^3}(1-qA\varrho/p_\varphi)(1+q\varrho^2(\partial A/\partial\varrho)p_\varphi) \qquad (26)$$

In an adiabatic process we have $d(\gamma\dot{\varrho})/dt \to 0$. Since the second expression in parentheses is zero before compression (see eq.(25), while the first cannot be zero in general, the adiabatic in-

variant is $\varrho^2 \partial A/\partial \varrho$. The second expression in parentheses is therefore written as $1-\varrho^2/\varrho_a^2$, where ϱ_a is the time dependent adiabatic value of ϱ.

To approximate the deviation of ϱ from its adiabatic value, it should be sufficient to consider the compression in an uniform field $B_z=B$, where $A=\varrho B/2$. Furthermore, we can assume $\gamma = 1$ for the ions. This yields from eqs. (25), (26):

$$\ddot{\varrho} = \frac{q^2 B_o^2 \varrho_o^4}{4 m_i^2 \varrho^3}(1-\varrho^4/\varrho_a^4) \tag{27}$$

Normalization according to $\sigma = \varrho/\varrho_o$, $\tau = t\omega_o$, where $\omega_o = qB_o/m_i$ is the initial cyclotron frequency and τ the initial revolution angle, leads to:

$$d^2\sigma/d\tau^2 = (1-\sigma^4/\sigma_a^4)/4\sigma^3 \tag{28}$$

Here σ_a is to be given as a time dependent function. When the compression is over and σ_a is constant again, eq. (28) can be shown to have the exact solution:

$$\sigma^2 = \lambda^2 + \alpha^2 + 2\lambda\alpha\cos(\tau/\sigma_a^2 + \delta) \tag{29}$$

where λ and α are constant like δ and related by:

$$\alpha^2 = \lambda^2 + \sigma_a^2 \tag{30}$$

This corresponds to a circular motion with radius $\alpha\varrho_o$, angular velocity ω_o/σ_a^2 whose centre is displaced by $\lambda\varrho_o$ from the initial centre. According to eq. (30) the ion energy may be greater, but can never be smaller than its adiabatic value. If $\lambda \ll \sigma_a$, we obtain from eqs. (29), (30) $\sigma \approx \sigma_a + \lambda\cos(\tau/\sigma_a^2 + \delta)$, where the second term is the nonadiabatic deviation from the final adiabatic value σ_a. Betatron oscillations are therefore produced around the final adiabatic radius. The oscillation amplitudes correspond to a radial emittance $\varepsilon \approx \pi\lambda^2\varrho_o/\sigma_a$.

Numerical values for α and λ are obtained from the maxima and minima of $\sigma(\tau)$ after the compression by numerically integrating eq. (28). To get somewhat realistic values, a radius compression by the factor 1/8 along an exponential decay curve was chosen according to:

$$\sigma_a = \begin{cases} 1 & \text{for} \quad \tau < 0 \\ (1/8)^{\tau/\tau_c} & \text{"} \quad 0 \leq \tau \leq \tau_c \\ 1/8 & \text{"} \quad \tau > \tau_c \end{cases} \tag{31}$$

Here $\tau_c = t_c \omega_o$ is the normalized compression time, i.e. $\tau_c = 2\pi$ corresponds to one revolution of the ions in the initial state or 1.4 µsec for our proton example. Under these conditions the following table was obtained for different normalized compression times τ_c:

τ_c	α/σ_a	λ/σ_a	$\lvert p \rvert$	ε/radcm	t_c/sec
10	1.0172	0.1863	0.1808	2.59E-01	2.23E-06
20	1.0051	0.1009	0.0991	7.60E-02	4.46E-06
30	1.0024	0.0698	0.0683	3.63E-02	6.68E-06
40	1.0014	0.0539	0.0520	2.17E-02	8.91E-06
50	1.0010	0.0442	0.0418	1.45E-02	1.11E-05
60	1.0007	0.0374	0.0347	1.04E-02	1.34E-05
70	1.0005	0.0328	0.0295	8.02E-03	1.56E-05
80	1.0004	0.0294	0.0256	6.44E-03	1.78E-05
90	1.0004	0.0265	0.0227	5.24E-03	2.01E-05
100	1.0003	0.0248	0.0205	4.60E-03	2.23E-05

Tab.1: Nonadiabatic deviations after ion compression.

Here α/σ_a and λ/σ_a are the relative values of the final cyclotron radius and the deviation of the gyration centre from the initial centre with respect to the final adiabatic radius (for p see below). For our proton example, where ϱ_o = 19 cm, the resulting emittance ε and the real compression time t_c are also given. As can be seen for t = 11 µsec, the cyclotron radius differs only by 0.1 % from its adiabatic value and the

displacement of its centre is 4.4 %. Since binding forces due to the electrons were not taken into account, the deviations should be even smaller and can therefore still be neglected. To get the same results for heavy multiply charged ions, the compression time must be increased proportionally to A/Z.

A treatment of the nonadiabatic compression in an uniform magnetic field using Cartesian coordinates and complex variables instead of cylindrical coordinates was given in [10]. Here it may be seen that eq. (30) is a direct consequence of the constancy of the generalized momentum. Furthermore, an approximate integral expression denoted by p is given whose absolute value should correspond to our value λ/σ_a. Evaluating these integrals for our compression sheme (31) yields $4\,|p|^2 = (si(b)-si(a))^2 + (Ci(b)-Ci(a))^2$, where si and Ci denote the integral sine and cosine respectively and $a = \tau_c/2\ln(8)$, $b=64a$. The values of $|p|$ are given in Table 1. As can be seen, there is good agreement with λ/σ_a.

3. Experiment

3.1 Experimental setup

The experimental setup (Fig. 2) consists of the ion source, the beam guiding system, and the vessel where the ions are injected into a closed orbit in a magnetic mirror field.

A duoplasmatron [11] with soft iron anode was used as ion source. It was supplied with cleaned H_2 at a pressure of 0.4 torr which was controlled by a variable leak valve. The ions are extracted from the duoplasmatron anode aperture by means of an extraction electrode. The anode and the extraction electrode are shaped as shown in Fig. 2 to form a Pierce-like geometry.

A voltage of -20 kV of the 140 cm long beam guiding system was chosen in order to reduce the beam diameter expansion due to space charge effects and beam emittance. An iron encased magnetic lens is used to direct the proton component of the beam to the injection snout. Electrical adjustment of possible astigmatism and position aberration of the beam is provided for by means of an electric quadrupole lens and a set of deflecting plates. In the region of the diffusion pump stud the beam guiding tube is replaced by a series of disk-shaped apertures in order to obtain a sufficient vacuum. Using a 2000 l/sec oil diffusion pump, a pressure of 5×10^{-5} torr was achieved. A pulse electrode described in Sec.3.22 was intended to serve as a beam chopper. In the last section a 50 cm long guiding tube made of soft iron shields the beam from the magnetic mirror field. The 8 cm diameter outer tube serves as a second magnetic shield. At the end of the beam guiding system, the beam is decelerated to the desired injection energy of 3.75 keV (see Sec. 3.4). In order to compensate for the strong refraction power of the decelerating immersion lens, a tungsten grid is inserted at the end of the outer pipe. The resulting refraction power can be adjusted mechanically by varying the position of the inner tube. The ion beam is injected into a glass vessel with an inner diameter of 50 cm. To avoid electrostatic charging, the vessel is coated with a thin grounded film of gold. Two pairs of series connected coils are arranged symmetrically to generate a magnetic mirror field. With the outer coils having 84 turns and the inner coils having 33 turns each, a field index of $n = 0.5$ was achieved on the orbit at a radius of 19 cm. The field on the orbit was 480 G with a coil current of 365 A. An electric inflector (see Sec. 2.4 and 3.4) is used to guide the beam straight on through the magnetic field to the apex of the orbit. To maintain a pressure below 2×10^{-5} torr, an additional 500 l/sec diffusion pump was attached to the vacuum vessel.

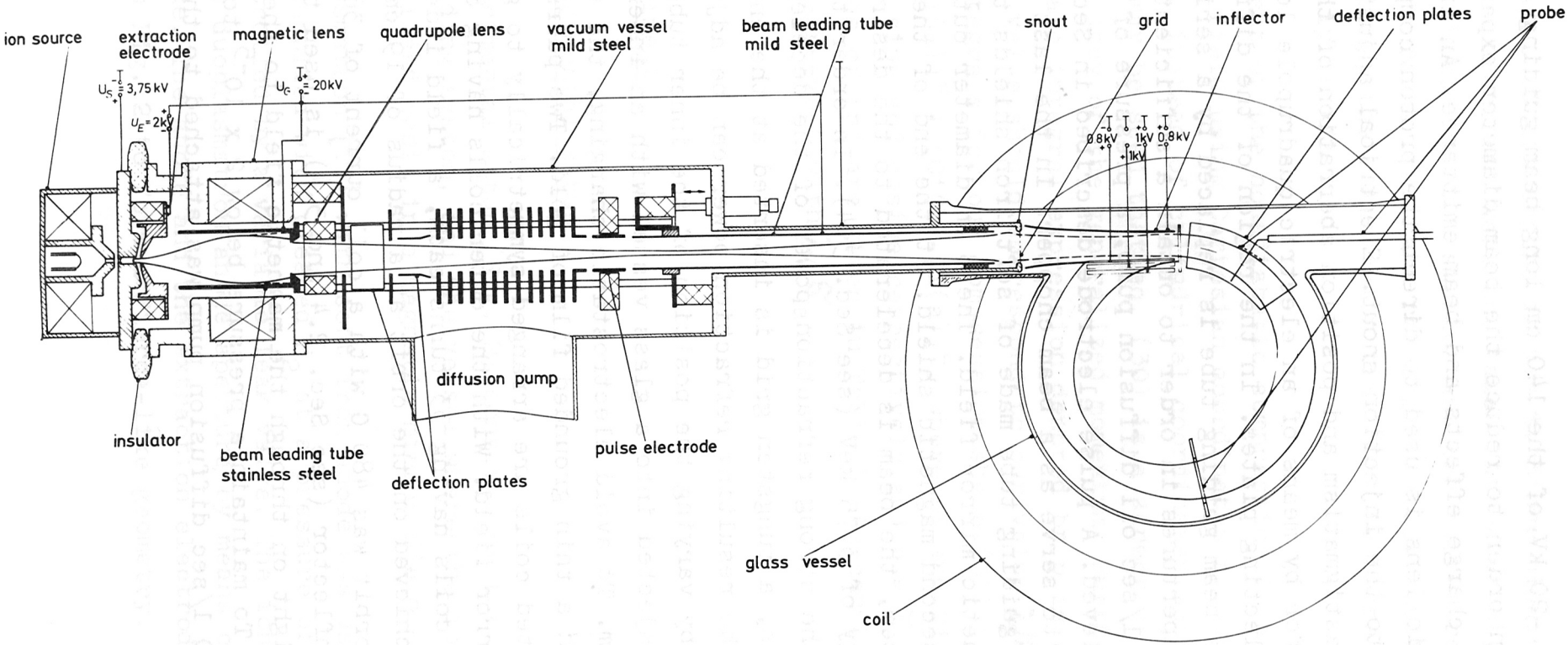

Fig. 2: Experimental setup

3.2 Systems for pulsed operation

3.21 Duoplasmatron pulsing

The H^+ efficiency of the duoplasmatron source can be improved by increasing the arc current to about 30 A. In steady state operation this current would cause excessive dissipation losses and undue loading of the power supply. Therefore a 10 msec pulse taken direct from the 50 Hz mains at the secondary of an insulating transformer is used. At near zero voltage a thyristor switch is triggered by a short pulse and closes the duoplasmatron cathode circuit. A sine half-wave is applied to the circuit. After 10 msec the voltage reverses sign and the switch returns to the non-conducting condition.

Because the duoplasmatron is at a potential of 3.75 kV to ground, high-impedance differential amplifiers were used to measure the source parameters arc voltage, arc current, auxiliary electrode current, and emission current. The imput resistance of 20 MΩ of the amplifiers allows the use of small coupling capacitors without distorting the signals.

3.22 Beam chopper

For some of our experiments we needed a square-wave ion beam pulse with a duration of 1.4 μsec. This is accomplished by a pulse electrode which is normally at a potential of 5 kV to reject the ion beam. The gate is opened by switching a 500 pF capacitor charged to -20 kV to the electrode by means of a pressurized spark gap. After 1.4 μsec a positively charged capacitor is switched on to close the gate again. The principle of operation is shown in Fig. 3. Short rise and fall times of the pulse can be achieved by minimizing the stray capacitance

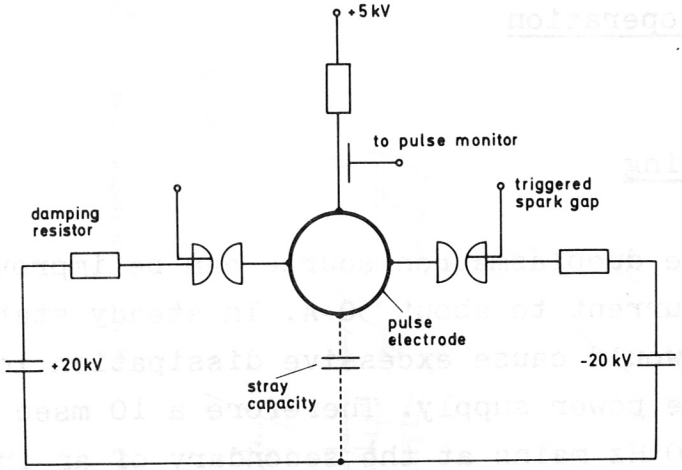

Fig. 3: Beam chopper circuit

of the chopper electrode and the inductance of the feeding line. By inserting two pulse generator capsules into our vacuum vessel we got slopes shorter than 100 nsec.

3.23 Inflector power supply

For our inflector system we used a power supply with 3 stabilized outputs for each polarity variable from 500 V to 1200 V. These voltages have to be switched to ground potential simultaneously in a time small compared with the revolution time of the ions to prevent the ion ring from being distorted during the second revolution. For this purpose we used a series connection of 3 thyristor switches for each polarity and achieved a switching time of 200 nsec.

3.24 Ring azimuthal irregularity probe

To detect the ion ring by its azimuthal irregularities, a wire probe was immersed in the orbit. The sensitivity of the probe was increased by a miniaturized transistor amplifier at the base of the probe.

3.25 Ion ring deflection

For measuring the number of particles of the ring we used a pair of deflection plates which directed the beam onto a target electrode. A 14 kV trigger device with externally attenuated output served as a deflection generator with a rise time shorter than 100 nsec. The ion current at the target was integrated by the capacity of the connecting cable to give a measure of the captured charge. In order to increase the sensitivity of the measurement, precharging of the cable by parasitic ions had to be compensated for by means of a reverse current.

3.26 Pulse-flow diagram

The combined action of the pulsed systems is shown in the pulse-flow diagram in Fig. 4. After the start of the cycle, the starting pulse is delayed for 0.5 sec to protect the duoplasmatron from being triggered too often. Then the duoplasmatron thyristor switch is triggered at the correct phase to give a 10 msec pulse. At the maximum of the duoplasmatron pulse, after 5 msec, the beam chopper is activated. The beam chopper is reset 1.4 µsec later to the beam rejecting voltage. After 0.8 µsec the trailing edge of the chopped ion beam has passed the inflector and the inflector voltage has to be switched off. Simultaneously or after a delay up to a few microseconds, the deflection plates are pulsed to measure the ring charge at various times. In the final experimental stage the beam chopper was omitted.

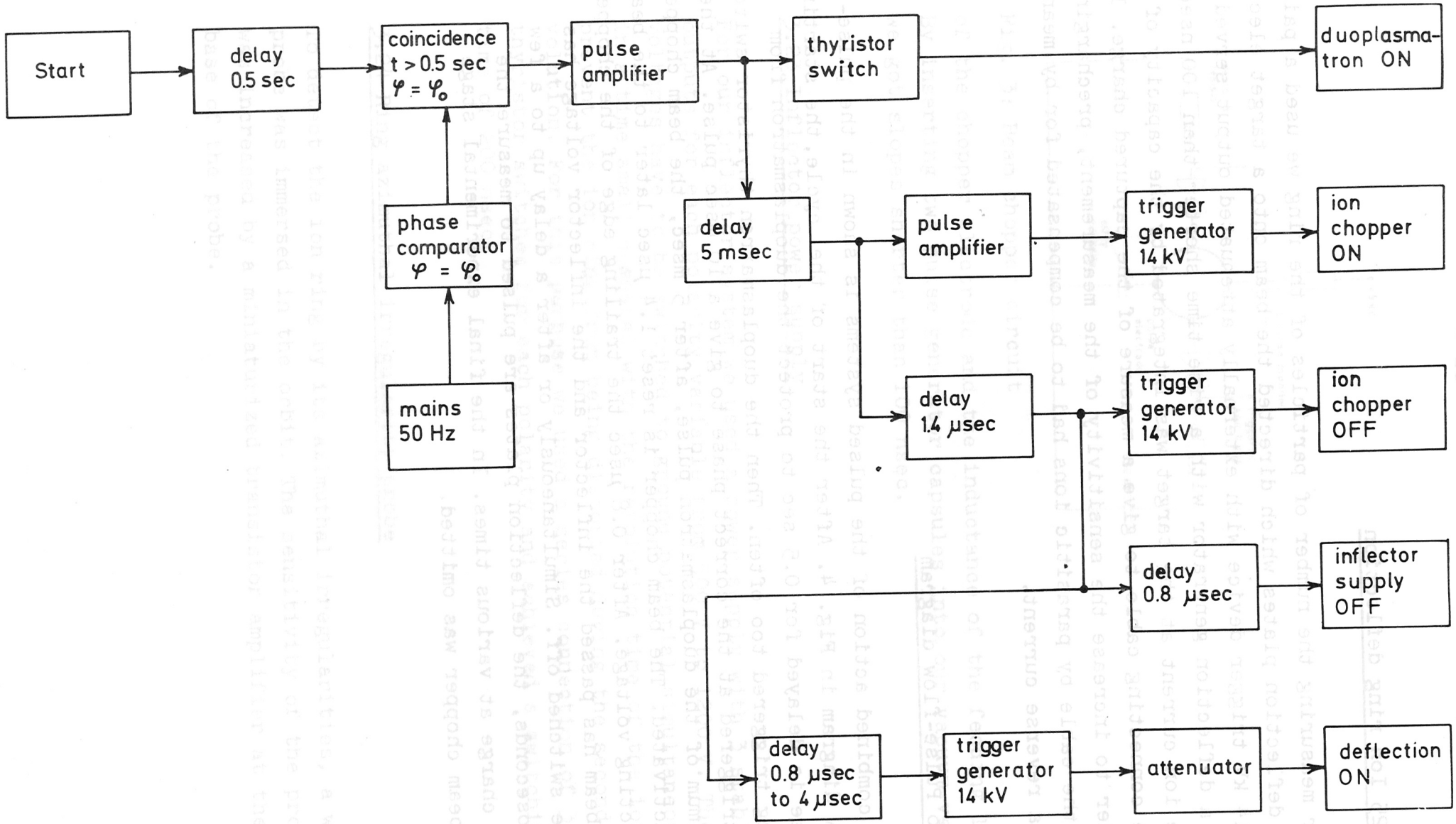

Fig. 4: Pulse-flow diagram

3.3 Emission properties of the ion source

Owing to the well-known fact that the proton emission of a duoplasmatron increases with higher arc current, single pulse operation at 30 A arc current as described in 3.21 was applied.

Further investigations were made in order to optimize the emission properties [12] . It was found that the emission current depends strongly on the static neutral gas pressure p_o in the duoplasmatron (Fig. 5). The emission has a maximum of 55 mA at a static pressure

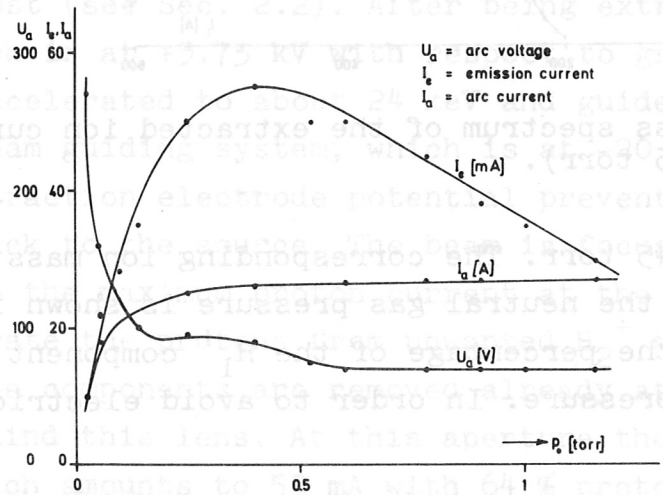

Fig.5: Pulse amplitudes of emission current, arc current, and arc voltage as functions of the H_2 pressure (p_o) applied to the duoplasmatron.

of 0.4 torr and decreases quickly with lower pressure values. The measured emission current is mainly an ion current because backward moving electrons are rejected by the extraction electrode, which was at a potential of -2 kV with respect to the beam guiding system (see Fig. 2).

The mass spectrum of the beam as a function of the neutral gas pressure in the anode region was measured with a probe situated inside a Faraday cup with an aperture of 3 cm diameter. In front of the aperture an electrode at extraction electrode potential prevents the fast electrons from entering the cup. The separation

of the different masses was done by varying the focal length of the magnetic lens. Figure 6 shows a typical mass spectrum

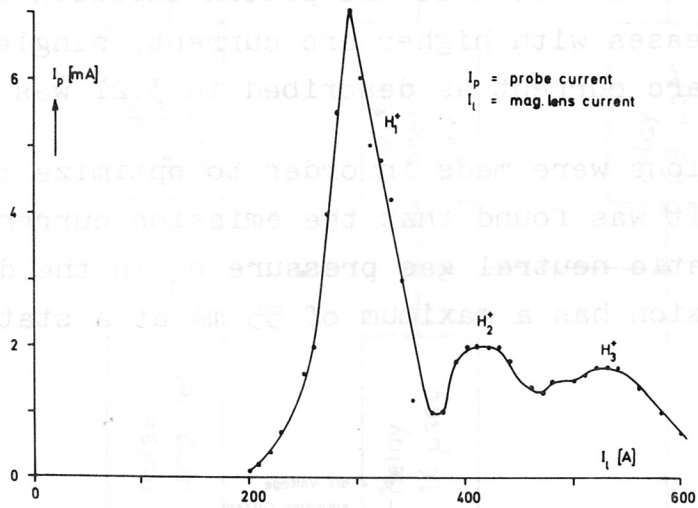

Fig.6: Mass spectrum of the extracted ion current (p_o = 0.45 torr).

taken at p_o = 0.45 torr. The corresponding ion mass distribution as a function of the neutral gas pressure is shown in Fig. 7. As can be seen, the percentage of the H_1^+ component increases with increasing pressure. In order to avoid electric breakdown

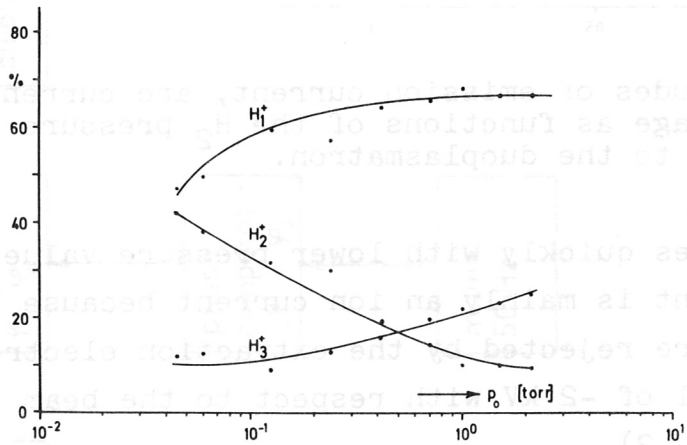

Fig. 7: Beam current composition

in the extraction gap and too high charge exchange in the beam guiding system, the source pressure has to be limited. A value of p_o = 0.5 torr was chosen, which combines maximum emission current with reasonable H_1^+ output at a sufficiently low leak

rate through the duoplasmatron emission aperture. With this adjustment the H_1^+ component contributed 66 % and the H_2^+ and H_3^+ components each contributed 17 % to the total emission current.

3.4 Beam guiding

As shown in Sec. 2.1, the protons have to be injected into the equilibrium orbit with an energy of 3.75 keV. At this low energy the beam spread in the guiding system between the source and the snout (see Fig.2) would be relatively high and most of the protons would get lost (see Sec. 2.2). After being extracted from the source, which is at +3.75 kV with respect to ground, they are therefore accelerated to about 24 keV and guided with this energy along the beam guiding system, which is at -20 kV. The more negative extraction electrode potential prevents electrons from streaming back to the source. The beam is focused by the magnetic lens to give the maximum proton current at the injection snout and to seperate the protons from unwanted H_2^+ and H_3^+ components. Most of these components are removed already at the 5 cm diameter aperture behind this lens. At this aperture the extracted ion current, which amounts to 55 mA with 64 % proton current, is largely reduced. In this way the residual beam emittance and the leak rate due to neutralized ions near the snout are reduced at the expense of a proton current reduction to 9 mA. A small part of the current reduction is due to charge exchange along the 137 cm long guiding system. With the charge exchange cross section of 4×10^{-16} cm^2 obtained for our conditions [13], the e-folding length was 1400 cm, yielding 9 % losses of the initial proton current.

Space charge compensation in the guiding system still seemed important in spite of the increased beam energy. This was concluded because the current at the snout was largely reduced

when short current pulses of one or two microseconds duration, as necessary for single-turn injection (see Sec. 3.6), were generated by means of the beam chopper (see Sec. 3.22). With an ionization cross section of the order of 10^{-16} cm^2 in our case [13] the build-up time for space charge compensation was more than 10 times larger than this pulse duration. For this reason the beam chopper, which was originally intended to improve measurements at the trapped ion ring by suppressing all unnecessary injection, was not used to a large extent. Little use has been made of the quadrupole lens and the deflecting plates (Fig.2) since the beam was sufficiently adjusted from the beginning.

As described in [5] , the emittance in the beam guiding system was found to be not larger than 200 mrad.cm for a 3 mA proton beam of 4 keV at a duoplasmatron arc current of 6 A. In accordance with [14] , the measurement employed a movable thin wire probe scanning the small proton beam bundles emerging behind a perforated disk hit by the beam. Measurements made in the ring seem to indicate higher final values (see Sec. 3.5).

At the injection snout the proton beam is decelerated to ground potential, i.e. to 3.75 keV, by a gauze lens (gauze at ground) whose focusing force is mechanically adjustable in a wide range. A focal length of about 8 cm proved appropriate in our case. For the gauze lens a tungsten grid with 0.25 mm spacing and 87 % transparency was mostly used. The aperture radius chosen at the injection snout for the trapping experiments was 2.3 cm, corresponding to the estimated minor equilibrium ring radius (see Sec. 2.3).

To reduce the magnetic field distortion at the equilibrium orbit below 2 %, the injection snout is drawn back 23 cm from the injection point, where the injector axis is tangential to the equilibrium orbit. In the intervening distance the beam is

guided by the electric inflector, whose operation and construction conditions are described in Sec. 2.4. The corresponding inflector electrode configuration is shown in Fig. 8. The top two plates are the actual inflector plates having about ± 800 V with respect to ground, the uppermost plate being negative. The lower plate is slotted half its length to allow multiple revolutions of the trapped ions. The electrodes below this plate correct the potential in the slot and below the inflector. Trapping is achieved by switching all electrodes to ground potential during injection as described in Sec. 3.6.

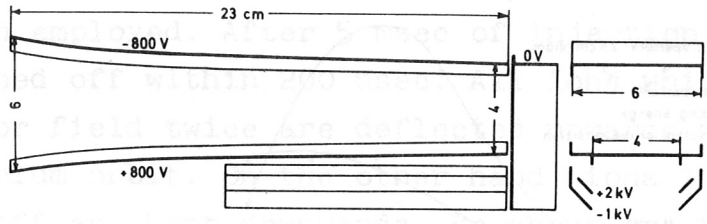

Fig. 8: Inflector electrode arrangement

3.5 Quality of the injected proton beam

During the 10 msec injection pulse (see Sec. 3.21) quasi-stationary measurements with constant inflector potentials were first made to investigate the quality of the proton current injected into the mirror field. For this purpose an azimuthally movable current probe 5 cm in diameter which was divided into 2 concentric parts of equal area, each part divided in turn into 4 equal segments, was used. The dependence of the probe currents on the azimuthal position α along the equilibrium orbit was measured for equal constant injection

energy of 3.75 keV in all cases, but for different beam guiding energies up to 24 keV and for two different aperture radii at the snout. Typical azimuthal current variations at the 3.4 cm diameter inner part of the probe are shown in Fig. 9. As can be seen, the azimuthal distance between the current maximum and minimum at the high beam guiding energy is somewhat more than 130°, which may be explained by collective betatron oscillations at our field index 0.5 (see eq.(7)) that produce variations of the current density. This type of collective oscillations seems to be produced mainly by spherical aberrations in the decelerating lens at the snout. This is concluded because

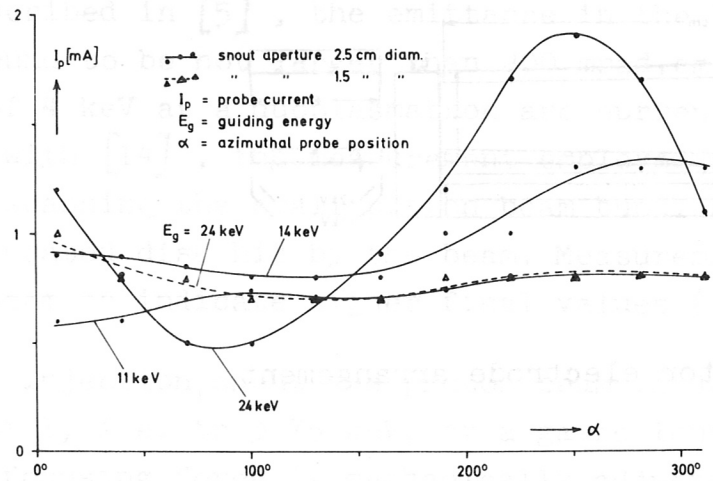

Fig.9: Angular current dependence measured at the azimuthally movable probe

a reduction of the beam guiding energy (reducing the lens action) as well as a reduction of the beam cross section at this lens reduces the azimuthal variation.

For optimum adjustment the azimuthal current minimum at our beam guiding energy of 24 keV could be increased to 1.4 mA and the maximum to 4 mA at the inner part of the probe. Since the equilibrium orbit radius is 19 cm, it may be concluded that more than this current minimum, but less than the maximum of about 4 mA is inside an emittance area of 340 mrad.cm. This effective increase of the emittance compared with earlier measurements (see Sec.3.4)

may be due to a higher emission temperature since the duoplasmatron arc current was increased in the meantime, to scattering at the gauze lens, and to emittance area deformations produced by spheric aberrations in this lens and by beam distortion in the inflector.

3.6 Trapping and detection of the ion ring

Originally it was planned to inject a chopped ion beam of 1.4 μsec duration. In this way a sufficient injection current could not be obtained owing to the fact that space charge compensation of the beam cannot build up in that short time (see Sec. 3.4). Therefore, a simplified method of using the inflector as a chopper as well has been employed. After 5 msec of injection the inflector voltages are turned off within 200 nsec. All ions which have passed the inflector field twice are deflected upwards with respect to the equilibrium orbit. On the other hand, ions injected after inflector switch off are bent downwards. So about one turn of injected ions remains on the orbit.

With the ring azimuthal irregularity probe described in Sec. 3.24 a periodic structure of the detected signal (Fig. 10) was observed. This signal is produced by azimuthal asymmetries of the gyrating

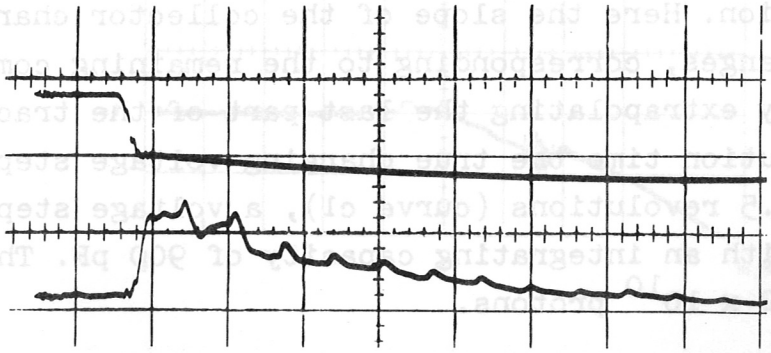

Fig. 10: Detection of the trapped ions;
upper trace, inflector switch off signal;
lower trace; trapped ring irregularity signal;
time, 2 μsec/div.

ion ring since only somewhat less than one turn can be trapped with our device. The period of 1.4 μsec corresponded to the expected revolution time on the orbit. About 15 periods could be detected, thus indicating 15 revolutions of the ring. The validity of the measurement was verified by results obtained at different injection energies with the magnetic field adjusted accordingly.

3.7 Measurement of the trapped ion number

To measure the number of protons trapped in the ring, they were deflected as described in Sec. 3.25 towards a collector. The deflector pulse could be delayed up to a few microseconds with respect to the inflector switch-off point in order to measure the trapped ion number at various times after inflection. Pre-charge compensation and integration of the signal as described in Sec. 3.25 was applied.

In Fig. 11 the collector charging is shown for protons which made about 1.5, 2.2 and 2.9 revolutions respectively in the magnetic field. As can be seen, charging begins about 0.4 μsec after the deflecting field is switched on, corresponding to the time of flight between deflecting plates and collector, and ends after one revolution. Here the slope of the collector charging trace suddenly changes, corresponding to the remaining compensation current. By extrapolating the last part of the traces back by the revolution time the true charging voltage step can be found. After 1.5 revolutions (curve c1), a voltage step of 2.2 V was found with an integrating capacity of 900 pF. This corresponds to 1.2×10^{10} protons.

When the deflector pulse was delayed by 1 and 2 microseconds (curves c2 and c3) respectively, the evaluation of the signals showed that the relative losses per revolution are nearly constant, being about 60 %. This high loss rate may be explained

by particle losses at the different electrodes and by charge exchange due to the high neutral gas pressure of 2 x 10^{-5} torr.

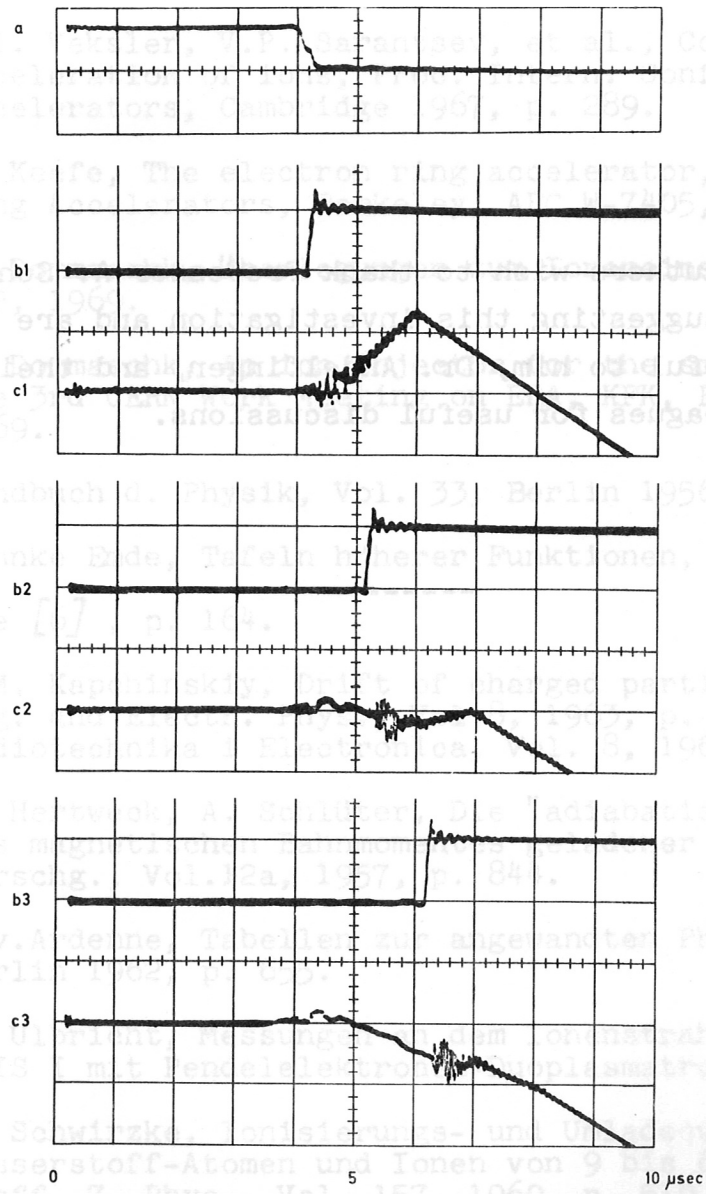

Fig.11: Measurement of the trapped proton number at different times after inflection; trace a, inflector voltage, b1 to b3, deflector voltage, c1 to c3, corresponding collector voltage (1V/div.); time, 1 µsec/div.

The authors wish to thank Professor A. Schlüter for suggesting this investigation and are also grateful to him, Dr. Andelfinger, and their colleagues for useful discussions.

---

4. References

[1] G.I.Budker, Relativistic stabilzed electron beam, CERN Symp. on High Energy Accelerators, 1956, p. 68.

[2] V.I. Veksler, V.P. Sarantsev, et al., Collective linear acceleration of ions, Proc. Intern. Conf. on High Energy Accelerators, Cambridge 1967, p. 289.

[3] D. Keefe, The electron ring accelerator, Symp. on Electron Ring Accelerators, Berkeley, AEC W-7405, Febr. 1968, p. 145.

[4] W. Dommaschk, Überlegungen zum Ioneneinschuss-Experiment, IPP, 1969.

[5] W. Dommaschk, An ion injector for the smokatron, Proc. of the 3rd CERN Work Meeting on ERA, KFK, Ext. Rep. 3/69-30, 1969.

[6] Handbuch d. Physik, Vol. 33, Berlin 1956, p. 24.

[7] Jahnke Emde, Tafeln höherer Funktionen, Leipzig 1948, p. 26.

[8] See [6] , p. 164.

[9] I.M. Kapchinskiy, Drift of charged particle beams, Radio Eng. and Electr. Phys., Vol.8, 1963, p. 987; Russ. orig., Radiotechnika i Electronica, Vol. 8, 1963, p. 985.

[10] F. Hertweck, A. Schlüter, Die "adiabatische Invarianz" des magnetischen Bahnmomentes geladener Teilchen, Z.Naturforschg., Vol.12a, 1957, p. 844.

[11] M.v.Ardenne, Tabellen zur angewandten Physik, Vol.1, Berlin 1962, p. 655.

[12] P. Ulbricht, Messungen an dem Ionenstrahl-Injektor-System ISIS I mit Pendelelektronen-Duoplasmatron, IPP 2/87, 1970.

[13] F. Schwirzke, Ionisierungs- und Umladequerschnitte von Wasserstoff-Atomen und Ionen von 9 bis 60 keV in Wasserstoff, Z. Phys., Vol. 157, 1960, p. 510.

[14] P.H. Rose, R.P. Bastide et al., Description of a device used to measure ion beam emittance, Rev. Sci. Instr., Vol.35, 1964, p. 1283.